HHS Public Access

Author manuscript

*Dev Biol*. Author manuscript; available in PMC 2024 September 01.

Published in final edited form as:

*Dev Biol*. 2023 September ; 501: 28–38. doi:10.1016/j.ydbio.2023.06.004.

# *Sall4* restricts glycolytic metabolism in limb buds through transcriptional regulation of glycolytic enzyme genes

**Hiroko Kawakami**[1,2,3], **Katherine Q. Chen**[1], **Ruizhi Zhang**[1], **Matthew P. Pappas**[1], **Abigail Bailey**[1], **Julie A. Reisz**[4], **Dylan Corcoran**[1], **Ryuichi Nishinakamura**[5], **Angelo D'Alessandro**[4], **Yasuhiko Kawakami, Ph.D.**[1,2,3]

[1:]Department of Genetics, Cell Biology and Development, University of Minnesota, Minneapolis, MN, United States of America

[2:]Stem Cell Institute, University of Minnesota, Minneapolis, MN, United States of America

[3:]Developmental Biology Center, University of Minnesota, Minneapolis, MN, United States of America

[4:]Department of Biochemistry and Molecular Genetics, University of Colorado Anschutz Medical Campus, Aurora, CO, United States of America

[5:]Department of Kidney Development, Institute of Molecular Embryology and Genetics, Kumamoto University, Kumamoto, Japan

## Abstract

Recent studies illustrate the importance of regulation of cellular metabolism, especially glycolysis and pathways branching from glycolysis, during vertebrate embryo development. For example, glycolysis generates cellular energy ATP. Glucose carbons are also directed to the pentose phosphate pathway, which is needed to sustain anabolic processes in the rapidly growing embryos. However, our understanding of the exact status of glycolytic metabolism as well as genes that regulate glycolytic metabolism are still incomplete. *Sall4* is a zinc finger transcription factor that

*Correspondence to: Yasuhiko Kawakami, Ph.D., Department of Genetics, Cell Biology and Development, 321 Church St. SE., 6-160 Jackson Hall, University of Minnesota, Minneapolis, MN. 55455, kawak005@umn.edu.

Declaration of competing interest

The authors have no competing interest.

**Figure S1 Heatmap with hierarchical clustering of the polar metabolomics results**

Relative levels of all metabolites obtained from the mass spectrometry assay is shown.

**Figure S2 Comparison of glycolytic metabolite levels in WT and *Sall4* cKO forelimb buds**

(A-I) Relative levels of intracellular glucose (A), hexose 6-phosphate (H6P, B), fructose 1,6-bisphosphate (FBP, C), glyceraldehyde 3-phosphate (G3P, D), bisphosphoglycerate (BPG, E), 2/3-Phospho-D-glycerate (PG, F), phosphoenol pyruvate (PEP, G), pyruvate (H), lactate (I) at E9.5 and E10.5.

(J, K) Ratios of pyruvate/phosphoenol pyruvate (J) and lactate/hexose 6-phosphate (K) at E9.5 and E10.5.

Each dot represents a sample, and bars show average ± standard deviation. Statistical test was performed by unpaired *t*-test and the p-values are shown in each panel.

**Figure S3 Comparison of TCA cycle metabolite levels in WT and *Sall4* cKO hindlimb buds** Relative levels of citrate (A), 2-oxoglutarate (2-OG, B), 2-oxoglutaramate (2-OGM, C), succinate (D), fumarate (E) malate (F), and 2-hydroxyglutarate/citramalate (2-HG, G) at E9.5 and E10.5. Each dot represents a sample, and bars show average ± standard deviation. The p-values are shown in each panel.

is highly expressed in undifferentiated cells in developing mouse embryos, such as blastocysts and the post-implantation epiblast. *TCre; Sall4* conditional knockout mouse embryos exhibit various defects in the posterior part of the body, including hindlimbs. Using transcriptomics approaches, we found that many genes encoding glycolytic enzymes are upregulated in the posterior trunk, including the hindlimb-forming region, of *Sall4* conditional knockout mouse embryos. In situ hybridization and qRT-PCR also confirmed upregulation of expression of several glycolytic genes in hindlimb buds. A fraction of those genes are bound by SALL4 at the promoters, gene bodies or distantly-located regions, suggesting that *Sall4* directly regulates expression of several glycolytic enzyme genes in hindlimb buds. To further gain insight into the metabolic status associated with the observed changes at the transcriptional level, we performed a comprehensive analysis of metabolite levels in limb buds in wild type and *Sall4* conditional knockout embryos by high-resolution mass spectrometry. We found that the levels of metabolic intermediates of glycolysis are lower, but glycolytic end-products pyruvate and lactate did not exhibit differences in *Sall4* conditional knockout hindlimb buds. The increased expression of glycolytic genes would have caused accelerated glycolytic flow, resulting in low levels of intermediates. This condition may have prevented intermediates from being re-directed to other pathways, such as the pentose phosphate pathway. Indeed, the change in glycolytic metabolite levels is associated with reduced levels of ATP and metabolites of the pentose phosphate pathway. To further test whether glycolysis regulates limb patterning downstream of *Sall4*, we conditionally inactivated *Hk2*, which encodes a rate-limiting enzyme gene in glycolysis and is regulated by *Sall4*. The *TCre; Hk2* conditional knockout hindlimb exhibited a short femur, and a lack of tibia and anterior digits in hindlimbs, which are defects similarly found in the *TCre; Sall4* conditional knockout. The similarity of skeletal defects in *Sall4* mutants and *Hk2* mutants suggests that regulation of glycolysis plays a role in hindlimb patterning. These data suggest that *Sall4* restricts glycolysis in limb buds and contributes to patterning and regulation of glucose carbon flow during development of limb buds.

## Graphical Abstract

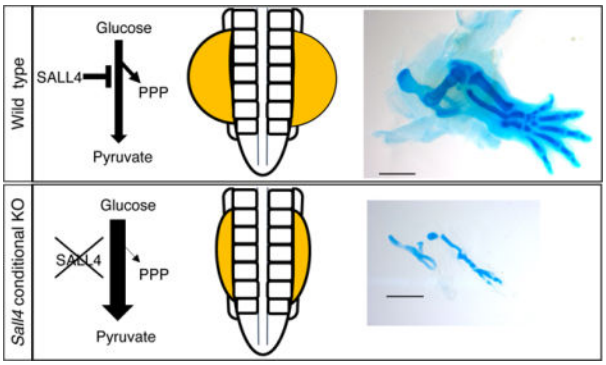


### Keywords

Limb bud; glycolysis; metabolite; cellular energy; TCA cycle; *Sall4*

## 1. Introduction

Embryonic development requires metabolic regulation to sustain the anabolic reactions that are essential to build macromolecules and, ultimately, biomass (Johnson et al., 2003). Studies in mammalian embryos demonstrated changes of energy metabolism and glycolysis during embryogenesis. Early pre-implantation embryos use glucose-derived pyruvate and lactate – byproducts of glycolysis - to feed the tricarboxylic acid (TCA) cycle to generate adenosine triphosphate (ATP) (Brinster, 1965). Pyruvate is derived from glycolysis or the external environment, and is used during preimplantation development (Lewis, 2015). At the blastocyst stage, pyruvate consumption decreases, glucose uptake is increased, and glycolytic activity elevates (Leese, 2012). The metabolic status of blastocysts is characterized by high levels of ATP production through glycolysis as well as increased conversion of pyruvate to lactate (Redel et al., 2012), which is called Warburg metabolism – a metabolic adaptation that leverages faster rates of ATP generation at the expense of incomplete glucose oxidation to provide triose carbon backbones to sustain anabolic reactions (Kukurugya and Titov, 2022; Vander Heiden et al., 2009). Clinically, early-stage metabolic adaptations in the developing blastocyst are amenable to monitoring via the blastocoele fluid in the context of in vitro fertilization approaches to determine blastocyst pre-implantation viability (D'Alessandro et al., 2012).

After implantation, vitelline circulation and chorioallantoic branching are established during the early organogenesis stage, which provides oxygen and nutrients from the maternal circulation (Arora and Papaioannou, 2012; McGrath et al., 2003). While oxidative phosphorylation replaces glycolysis as an efficient system for glucose-derived carbon oxidation (Miyazawa et al., 2017; Solmonson et al., 2022) (in terms of full glucose-derived carbon oxidation, but not net energy production (Kukurugya and Titov, 2022)), regulation of glycolysis still plays an important role for rapidly growing embryos. Specifically, it has been demonstrated that levels of intracellular glucose metabolites downstream of phosphofructokinase decrease, while levels of pyruvate increase from E8.5 to E10.5 (Miyazawa et al., 2017). This change is driven by the reduced activities of key glycolytic enzymes, phosphofructokinase and aldolase, which direct glucose carbon flow to the pentose phosphate pathway. Re-directed carbon is used for anabolic processes to produce biomass and reducing power (NADPH) for proliferating cells (DeBerardinis et al., 2008; Palsson-McDermott and O'Neill, 2013; Patra and Hay, 2014).

Other recent studies demonstrated the roles of the spatially controlled glycolysis gradient in tissue patterning in chick and mouse embryos. In the presomitic mesoderm, the unsegmented paraxial mesoderm at the posterior end of the elongating body, a posterior high – anterior low glycolytic activity gradient regulates cell differentiation in both chick and mouse embryos (Bulusu et al., 2017; Oginuma et al., 2017). Furthermore, higher levels of glycolysis at the posterior part of the presomitic mesoderm activates ß-catenin signaling, which promotes mesodermal differentiation form neuromesodermal progenitors (Oginuma et al., 2020). Despite these advances in understanding the status and roles of glycolysis in post-gastrulation embryos, our understanding of the glycolytic metabolic status and its roles in post-gastrulation embryos are still incomplete.

*Sall4* encodes a transcription factor with multiple zinc finger domains (de Celis and Barrio, 2009; Sweetman and Munsterberg, 2006) involved in the maintenance of undifferentiated cell phenotypes in mouse embryonic stem cells (Miller et al., 2016; Ru et al., 2022; Zhang et al., 2006). Several studies provided evidence that SALL4 acts as a transcriptional repressor through two mechanisms. The N-terminus of SALL4 interacts with the nucleosome remodeling and deacetylase (NuRD) co-repressor complex and can facilitate transcriptional repression (Lu et al., 2009). In addition, a zinc finger cluster of SALL4 binds to AT-rich sequences in putative regulatory elements and represses neural gene expression in mouse embryonic stem cells (Miller et al., 2016; Pantier et al., 2021). *Sall4* is highly expressed in undifferentiated cells in developing mouse embryos, such as blastocysts and the post-implantation epiblast (Akiyama et al., 2015; Elling et al., 2006; Kohlhase et al., 2002; Sakaki-Yumoto et al., 2006; Tahara et al., 2018; Tsubooka et al., 2009; Xu et al., 2017). During development of post-gastrulation stages, *Sall4* expression rapidly deceases, but is maintained in the posterior part of the body and distal limb buds (Akiyama et al., 2015; Kohlhase et al., 2002; Tahara et al., 2018). Other than recent studies in human cancer cells on glycolysis (Shao et al., 2020) and oxidative phosphorylation (Tan et al., 2019), whether *Sall4* is involved in cell metabolism remains unknown. Conditional knockout (cKO) of *Sall4* by the *TCre* driver caused severe skeletal defects in the hindlimb and posterior axial skeleton (Akiyama et al., 2015; Tahara et al., 2019).

In this study, we revisited our published RNA-seq data comparing the posterior trunk tissues from wild type (WT) and *TCre; Sall4* cKO embryos (Tahara et al., 2019). We found that genes encoding glycolytic enzymes are upregulated in *Sall4* cKO embryos. Through comprehensive metabolite analysis of limb progenitor cells and limb bud cells in WT and *Sall4* cKO embryos by mass spectrometry, we found that glycolytic metabolite levels are lower and end-products pyruvate and lactate ratios to earlier glycolytic intermediates are higher in *Sall4* cKO hindlimb buds. Moreover, conditionally knocking out *Hk2*, which encodes a rate limiting glycolytic enzyme, phenocopied *Sall4* cKO hindlimb defects. Our results support the idea that glycolysis is accelerated in *Sall4* cKO embryos. Together with our observation that SALL4 is enriched on many of the glycolytic enzyme genes that are upregulated in *Sall4* cKO embryos, our results suggest that *Sall4* restricts glycolysis in the limb progenitor cells and the limb bud cells for hindlimb growth and patterning.

## 2. Materials and Methods

### 2.1. Animal breeding

Embryos for in situ hybridization were collected by timed mating of $Sall4^{fl/fl}$ females and $TCre^{Tg/Tg}; Sall4^{fl/+}$ males (Akiyama et al., 2015). After fixation in 4% paraformaldehyde in PBS + 0.1%Tween 20 overnight, embryos were washed and dehydrated in graded series of PBS + 0.1%Tween 20/methanol and stored in 100% methanol. $Hk2^{fl}$ mice (Patra et al., 2013) were crossed with *TCre* mice (Perantoni et al., 2005), and embryos were collected from the timed mating of $Hk2^{fl/fl}$ females and $TCre^{Tg/+}; Hk2^{fl/+}$ males. For skeletal analysis, embryos at E14.5 or E15.5 were collected and fixed in 50% ethanol and processed for Alcian Blue staining as previously described (Akiyama et al., 2015). Animal breeding was

performed according to the approval by the Institutional Animal Care and Use Committee of the University of Minnesota.

### 2.2. Whole mount in situ hybridization

Whole mount in situ hybridization was performed as previously described (Akiyama et al., 2015). Three to five embryos per probe per stage were examined. Partial sequences of glycolytic enzyme genes were amplified by RT-PCR (Table S1) and cloned in pGEM-T EASY (Promega). The sequence of each clone was confirmed by Sanger sequencing. The *Aldoa* probe is described previously (Miyazawa et al., 2017).

### 2.3. Metabolite analysis

Mouse embryos at E10.5 were dissected in cold PBS, and limb buds were manually dissected from the trunk with fine forceps and collected in cold PBS. Forelimb buds from E9.5–9.75 embryos were collected similarly. The E9.5–9.75 posterior tissue was dissected from the embryo by cutting at the $24^{th}$ – $25^{th}$ somite boundary, and the neural tissue was removed as previously described (Tahara et al., 2019). For simplicity, we refer to this mesoderm-enriched posterior trunk tissue as E9.5 hindlimb buds in this study. After removing PBS, the tissue was snap frozen, stored in liquid nitrogen, and shipped to the University of Colorado on dry ice.

Frozen specimens were weighed then metabolites were extracted using ice-cold methanol:acetonitrile:water (5:3:2, v:v:v) at 15 mg/mL in the presence of GB10 (Next Advance) glass beads. Samples were homogenized in a Bullet Blender (Next Advance, Troy, NY, USA) for 5 minutes at setting 4 and 4°C then vortexed vigorously for 30 min at 4 °C. Insoluble material was pelleted via centrifugation at 18,000 g for 10 min at 4 °C, and supernatants were analyzed by UHPLC-MS.

### 2.4 UHPLC-MS Analysis

High throughput metabolomics analyses were performed as previously described in detail using a Thermo Vanquish UHPLC (San Jose, CA, USA) coupled online to a Thermo Q Exactive mass spectrometer (Bremen, Germany) (Nemkov et al., 2019). Extracts (10 µL) were randomized then resolved over a Kinetex C18 column, 2.1 × 150 mm, 1.7 µm (Phenomenex, Torrance, CA, USA) with a 5 min gradient in positive and negative ion modes (separate runs) exactly as described (Nemkov et al., 2019). The Q Exactive MS scanned in Full MS mode from 65 to 950 m/z at 70,000 resolution with 4 kV spray voltage (ESI), 45 sheath gas, and 15 auxiliary gas. A technical mixture was injected after every 15 runs to verify instrument performance. Acquired data was converted from .raw to .mzXML file format using RawConverter. Metabolites were assigned and peaks integrated using Maven (Princeton, NJ, USA) in conjunction with the KEGG database.

### 2.5 Statistical test

Statistical examination of relative metabolite levels was performed by unpaired *t*-test. The heat map of all metabolites in Fig. S1 was constructed by GENE-E (Broad Institute). Graphs in figures were drawn by Prism software (GraphPad Software).

### 2.6 RNA-seq and ChIP-seq data analysis

RNA-seq data was obtained from the Sequence Read Archive database (BioProject accession number PRJNA525663). The analysis used the previously published CHURP pipeline (https://doi.org/10.1145/3332186.3333156). Briefly, after quality control with fastQC, and reads trimming with Trimmomatic (Bolger et al., 2014), reads were aligned to the GRCm38 genome by Hisat2 (Kim et al., 2019). Aligned reads were sorted with SAMtools (Danecek et al., 2021) and gene counts were determined with featureCounts (Liao et al., 2014). Differential expression testing with edgeR revealed differentially expressed genes (Robinson et al., 2010). GO analysis was performed using PANTHER (Mi et al., 2019; Thomas et al., 2022). SALl4 ChIP-seq data was obtained from the Sequence Read Archive database (BioProject accession number PRJNA525663). Reads were mapped to the mm10 genome with Bowtie2 (Langmead and Salzberg, 2012), and potential PCR duplicates were removed with Samtools rmdup (Danecek et al., 2021). Peaks were called on replicates with Macs2 (Jeon et al., 2020) and binding enrichment testing was done with DiffBind (Ross-Innes et al., 2012).

### 2.7 Quantitative RT-PCR analysis

Hindlimb buds from WT or *Sall4* cKO embryos at E10.5 were manually dissected using fine forceps and a carbon steel scalpel (No. 1316–14, Fine Science Tools). Total RNA was isolated using the Direct-zol RNA MicroPrep kit (Zymo Research) and cDNA was synthesized using iScript cDNA synthesis kit (BioRad) according to the manufacturers' instructions. qPCR was performed using SYBR green master mix (ThermoFisher) and primers in Table S2.

## 3. Results

### 3.1. Upregulation of expression of glycolytic enzyme genes in *Sall4* cKO embryos

In order to understand the roles of *Sall4* in post-implantation embryo development, we revisited our RNA-seq data, obtained from the trunk tissue posterior to the 24/25 somite levels (Tahara et al., 2019). Using gene ontology (GO) analysis of differentially expressed genes between WT and *Sall4* cKO embryos, we noticed that glucose metabolism is overrepresented (Fig. 1A). Specifically, the glucose catabolic process (GO:0006007), hexose catabolic process (GO:0019320), and regulation of glucose import (GO:0046324) exhibited 2.05–3.21 fold enrichment, which are comparable to the 2.78 and 2.24 fold enrichment of hindlimb morphogenesis (GO:0035137) and limb development (GO:0060173), respectively. Therefore, we looked at genes involved in glycolysis and found that they exhibited upregulation in *Sall4* cKO embryos (Fig. 1B). These genes include *Slc2a1* and *Slc2a3*, encoding glucose transporter-1 and glucose transporter-3, respectively. They also include genes encoding hexokinase (*Hk1*, *Hk2*), phosphofluctokinase (*Pfkp*, *Pfkl*) and pyruvate kinase (*Pkm*), which catalyze rate-limiting steps of glycolysis. Moreover, genes encoding other enzymes in the glycolytic pathway are also upregulated in *Sall4* cKO embryos, which include glucose 6-phosphate isomerase (*Gpi1*), aldolases (*Aldoa*, *Aldoc*), triosephosphate isomerase (*Tpi1*), glyceraldehyde 3-phosphate dehydrogenase (*Gapdh*), phosphoglycerate kinase (*Pgk1*), phosphoglycerate mutase 1 (*Pgam1*), and enolase (*Eno1*) (Fig. 1). Pyruvate is converted into lactate by lactate dehydrogenase, which consists of combinations of two

subunits, which are encoded by *Ldha* and *Ldhb*. In *Sall4* cKO, *Ldha* was upregulated, while *Ldhb* was downregulated. Lactate can be extruded from cells by the action of monocarboxylate transporter 4, encoded by *Slc16a3*, whose expression was also upregulated in *Sall4* cKO. Pyruvate, together with $NAD^+$ and coenzyme A, is also converted into acetyl-CoA by the pyruvate dehydrogenase complex. *Pdhb*, encoding pyruvate dehydrogenase (lipoamide) beta, was downregulated in *Sall4* cKO. *Pdk1*, encoding pyruvate dehydrogenase kinase, which inactivates pyruvate dehydrogenase by phosphorylating it, was upregulated in *Sall4* cKO.

To gain insight into whether *Sall4* may directly regulate these genes, we also re-visited our SALL4 ChIP-seq data obtained from the E9.5 posterior trunk mesoderm (Tahara et al., 2019). SALL4 is enriched within 1,000 bp upstream to +100 bp of transcription start sites (TSS) of *Slc2a1*, *Slc2a3*, *Aldoc*, *Pgk1*, *Pgam1*, *Eno1*, *Pkm*, and *Pdk1* (Fig. 1C, Table S3). SALL4 enrichment was also observed in distantly upstream regions (*Hk2*, *Pfkl*, *Gpi1*, *Ldhb*) or in the gene bodies (*Hk1*, *Hk2*, *Gpi1*, *Pfkl*, *Pfkp*, *Aldoa*, *Pkm*, *Ldha*, *Ldhb*, *Pdha*, *Pdhx*, *Slc16a3*). These results suggest that *Sall4* represses expression of glycolysis enzyme genes through binding to those genes.

### 3.2. Upregulation of glycolysis enzyme genes by whole mount in situ hybridization

We further examined expression patterns of several glycolytic genes by whole mount in situ hybridization at E9.5 and E10.5. Since glycolysis is a fundamental metabolic process, many genes are broadly expressed at E9.5, including in the hindlimb forming region. Expression patterns of *Gpi1*, *Pgk1*, *Eno1* and *Pkm* were comparable in WT and *Sall4* cKO at E9.5 as detected by in situ hybridization; however, *Hk2*, *Pfkl*, *Aldoa*, *Tpi1*, *Ldha* and *Pdk1* exhibited stronger signals in the hindlimb-forming region (Fig. 2A–J'). The overall expression patterns at E9.5 are consistent with RNA-seq data (Fig. 2A"-J") and showed upregulation of glycolytic gene expression in the hindlimb forming region. At E10.5, several genes showed localized expression patterns in WT. Specifically, *Tpi1* expression is stronger in the anterior and posterior margin of the hindlimb bud (Fig. 2O); *Eno1* and *Ldha* exhibited stronger signals in the distal periphery of the hindlimb bud (Fig. 2Q, S); *Pdk1* signals are stronger in the proximal part than distal part (Fig. 2T). In *Sall4* cKO embryos, the glycolytic genes examined exhibit stronger signals in the hindlimb bud than WT by in situ hybridization (Fig. 2K'-T'). To further confirm changes of expression levels at E10.5, we performed qRT-PCR analysis using RNA isolated from hindlimb buds (Fig. 2K"-T"). The results showed significant upregulation of these genes at E10.5 ($p<0.05$ by *t*-test) except *Ldha* (Fig. 2S"). The greater degree of variation in relative gene expression in *Sall4* cKO hindlimb buds may be derived from morphologically perturbed hindlimb buds at this stage. These results support the idea that *Sall4* represses glycolytic enzyme gene expression during early phase of limb development.

### 3.3. Global analysis of metabolites in limb buds between WT and *Sall4* cKO embryos

To further examine glycolysis status at E9.5 and E10.5, we performed high throughput global metabolomics by mass spectrometry (Nemkov et al., 2019). For this analysis, we prepared forelimb buds and hindlimb buds from E9.5 and E10.5 embryos, from WT and

*Sall4* cKO embryos. In the global analysis, relative quantification was utilized to establish comparative profiles of the polar metabolome (Table S4, Fig. S1).

Since the glycolytic pathway is linked to the TCA cycle and energy metabolism, we focused our analysis on metabolites of glycolysis, the TCA cycle, and energy-related nucleotides among others (Fig. 3). The heatmap shows overall clustering of samples with the same tissue and same genotype. In WT, these metabolite levels are higher at E10.5 than E9.5 in forelimb buds and hindlimb buds. In particular, TCA cycle metabolite levels increase from E9.5 to E10.5 in WT in forelimb buds and hindlimb buds. This is consistent with a recent finding that showed upregulation of TCA cycle metabolites in whole embryos from E8.5 to E10.5 (Miyazawa et al., 2017). In *Sall4* cKO, overall metabolite levels also seem to be higher at E10.5 than E9.5 in forelimb buds; however, the elevation of metabolite levels does not appear to be significant in hindlimb buds. When WT and *Sall4* cKO are compared, metabolite levels appear to be lower in *Sall4* cKO than WT at E9.5. The same trend is the case in hindlimb buds but not in forelimb buds at E10.5.

### 3.4. Reduced levels of glycolytic intermediate metabolites in *Sall4* cKO hindlimb buds

Given that expression of glycolytic enzyme genes is elevated in *Sall4* cKO in hindlimb forming region at E9.5 and in hindlimb buds at E10.5 (Fig. 2), we compared metabolite levels in WT and *Sall4* cKO within the same tissues at the same stage. In E9.5 hindlimb buds and in E10.5 hindlimb buds, intracellular glucose levels were comparable between WT and *Sall4* cKO samples. However, intermediate metabolite levels were consistently lower in *Sall4* cKO in both E9.5 and E10.5 samples (Fig. 4A–G). Specifically, levels of fructose bisphosphate (FBP), bisphosphoglycerate (BPG), phosphoglycerate (PG), and phosphoenolpyruvate (PEP) were reduced in *Sall4* cKO compared to WT, except for BPG in E9.5 and PG in E10.5. In contrast, the levels of pyruvate and lactate were comparable between WT and *Sall4* cKO in E9.5 hindlimb and E10.5 hindlimb samples (Fig. 4H, I). In forelimb buds, most of glycolytic intermediate levels did not show a significant difference between WT and *Sall4* cKO (Fig. S2). Specifically, only levels of intracellular glucose and pyruvate exhibited lower and higher levels, respectively, in *Sall4* cKO than in WT at E10.5 (Fig. S2A, H). These results, together with elevated expression of glycolytic enzyme genes, suggest that glycolytic metabolic flow is accelerated in *Sall4* cKO hindlimb cells. Importantly, end-product ratios to earlier glycolytic intermediates are higher in *Sall4* cKO hindlimb. Specifically, the pyruvate/PEP ratio and the lactate/hexose 6-phosphate (H6P, glucose 6-phosphate and fructose 6-phosphate) ratio are significantly elevated at E9.5 and E10.5, respectively, in *Sall4* cKO hindlimbs (Fig. 4J, K). The elevated ratios further support the idea that glycolytic metabolic flow is accelerated in *Sall4* cKO hindlimb cells. Given that *Sall4* cKO mutants exhibit skeletal defects specifically in the hindlimb, observed reduction of glycolytic metabolites may be related to the skeletal phenotype.

### 3.5. TCA cycle metabolite levels are comparable between WT and *Sall4* cKO hindlimb buds

Compared to glycolysis metabolites, the levels of TCA cycle metabolites are comparable between WT and *Sall4* cKO hindlimb buds (Fig. 3, Fig. S3). Specifically, the levels of citrate, 2-oxoglutarate, 2-oxoglutaramate, succinate, fumarate, malate, and 2-

hydroxyglutarate/citramalate did not show significant differences at E9.5 and E10.5, except that the p-value for 2-hydroxyglutarate at E10.5 was 0.050.

### 3.6. Reduced ATP levels in *Sall4* cKO hindlimb buds

Pyruvate can be converted into acetyl-CoA and used in the TCA cycle, which generates ATP and $NAD^+$. Pyruvate can also be reduced to lactate, which regenerates $NAD^+$ from NADH. The RNA-seq data showed reduced expression of *Pdhb* and increased expression of *Pdk1* (Fig. 1), which suggested reduction in generation of acetyl-CoA from pyruvate. In contrast, *Ldha* and *Slc16a3* were upregulated, which suggests increased conversion of pyruvate to lactate and exclusion of lactate. In our mass spectrometry analysis, acetyl-CoA was undetectable, and lactate levels and $NAD^+$ levels were comparable in hindlimbs between WT and *Sall4* cKO at E9.5 and E10.5 (Fig. 4I, 5A). In contrast, ATP levels were reduced in *Sall4* cKO, although the p-value at E9.5 was 0.051 (Fig. 5B). These results suggest that pyruvate may be preferentially converted into lactate, which might be excluded from the cells, rather than generating acetyl-CoA to feed the TCA cycle in hindlimb buds.

### 3.7. Reduction of 6-phosphogluconate levels in *Sall4* cKO hindlimb buds

It has been reported that glucose carbon flow is directed to the pentose phosphate pathway (PPP) in the stage we examined (Miyazawa et al., 2017). Although we did not obtain full coverage of the PPP (Table S3), 6-phosphogluconate, sedoheptulose phosphate, and ribose phosphate were detected. Among them, the level of 6-phosphogluconate was significantly lower in *Sall4* cKO hindlimb buds, compared to WT hindlimb buds, both at E9.5 and E10.5 (Fig. 5C). Moreover, the 6-phosphogluconate ratio to an earlier intermediate H6P is lower in the *Sall4* cKO hindlimb (Fig. 5D). This data suggests that glucose carbon flow into the pentose phosphate pathway is impaired in *Sall4* cKO hindlimb buds.

### 3.8. *TCre; Hk2* conditional knockout phenocopied *TCre; Sall4* hindlimb defects

Our data show that *Sall4* negatively regulates expression of glycolytic enzyme genes (Fig. 1, 2, Table S2), among which HK2 catalyzes the first reaction of the glycolysis pathway. In order to further assess the role of glycolysis, we conditionally inactivated *Hk2* by *TCre*. A previous study showed that $Hk2^{-/-}$ embryos were retarded in growth around E7.5-E8.5 (Heikkinen et al., 1999). In contrast, we were able to recover *Hk2* cKO embryos at E14.5–15.5, which exhibited smaller bodies than either WT or littermate controls ($TCre^{+/+}; Hk2^{fl/+}$, $TCre^{+/+}; Hk2^{fl/fl}$, $TCre^{Tg/+}; Hk2^{fl/+}$) (Fig. 6A, B). The *Hk2* cKO hindlimb skeleton exhibited a hypoplasic pelvic girdle, small cartilage condensation at the position of femur, and loss of tibia and anterior digits (Fig. 6E, F, Table 1). They also exhibited loss of posterior digits in half of the forelimbs examined in this study (Fig. 6C, D, Table 1). These data demonstrate the requirement of *Hk2* for proper hindlimb skeletal patterning. The hindlimb skeletal defects in *Hk2* cKO embryos are similar to the defects of proximal-anterior skeletal elements in *TCre; Sall4* cKO hindlimbs (Fig. 6G) (Akiyama et al., 2015). Since *Sall4* regulates *Hk2* expression (Fig. 1, 2, Table S3), our data provides genetic evidence that *Sall4* regulation of glycolysis controls limb skeletal patterning.

## 4. Discussion

Cellular metabolism supports development by multiple mechanisms. These include supplying metabolic intermediates for the synthesis of macromolecules, energy production, and epigenetic regulation (Gándara and Wappner, 2018; Lu and Thompson, 2012). Compared to pre-implantation embryos, the detailed metabolic status of post-implantation embryos is only just starting to be understood. Recent studies revealed detailed status of changes in glycolytic metabolite levels in the whole embryo (Miyazawa et al., 2017) or in the presomitic mesoderm (Bulusu et al., 2017; Oginuma et al., 2017); however, metabolite levels in developing limb buds have not been studied. Our comprehensive metabolite profiling by mass spectrometry is the first report of the status of metabolism in forelimb buds and hindlimb buds during early outgrowth stages in limb development.

### Accelerated glycolysis and failure to re-direct carbon flow to the pentose phosphate pathway in *Sall4* cKO hindlimb buds

Re-visiting our RNA-seq data and SALL4 ChIP-seq data provided a striking display of upregulation for glycolytic gene expression in *Sall4* cKO embryos. The data suggests that SALL4 directly represses many glycolytic enzyme genes. In situ hybridization data and qRT-PCR analysis also supported this notion. Regarding glycolytic metabolites, many glycolytic intermediate metabolites exhibited reduced levels in *Sall4* cKO hindlimb buds, but not in forelimb buds. Elevated expression of glycolytic enzyme genes would have caused accelerated glycolytic metabolism that would give rise to a rapid flow of glucose to pyruvate and reduced intermediate metabolite levels. The elevated end-product ratios of pyruvate and lactate compared to earlier glycolytic intermediates also support this idea. This condition might prevent re-directing glucose carbon flow to the pentose phosphate pathway, which is consistent with reduced levels of 6-phosphogluconate in *Sall4* cKO hindlimb buds. Our previous analysis showed reduced proliferation of mesenchyme cells in *Sall4* cKO hindlimb buds and tails (Akiyama et al., 2015; Tahara et al., 2019), which could contribute to small hindlimb buds and tail truncation in *Sall4* cKO. The glucose carbon, directed to the PPP, is used in biomass production and maintenance of the redox balance to support rapidly growing embryos (Patra and Hay, 2014; Yamamoto et al., 2014). The failure to direct glucose carbon flow to the PPP by accelerated glycolytic flow in *Sall4* cKO hindlimbs may also underlie the small size of hindlimb buds and posterior body truncation in *Sall4* cKO embryos.

The reduced expression of *Pdhb* and increased expression of *Pdk1* in *Sall4* cKO embryos in the RNA-seq data and qRT-PCR data suggests that the use of pyruvate for the TCA cycle may be restricted in *Sall4* cKO. Given that *Ldha* and *Slc16a3* are concomitantly upregulated in the RNA-seq data, we speculate that pyruvate is preferentially converted to lactate and excreted from the cell in *Sall4* cKO hindlimb buds. Taken together, we propose that *Sall4* restricts glycolysis, which contributes to directing glucose carbons to the PPP and generating proper energy levels for rapidly proliferating cells in hindlimb buds.

### Glycolysis and hindlimb development

Our previous studies have shown that transcription factors, such as those encoded by *Plzf*, *Gli3* and *Hox* genes, regulate hindlimb skeletal pattern downstream of *Sall4* (Akiyama et al., 2015; Chen et al., 2020). In addition to the transcriptional network involving these genes, our current study supports the idea that glycolysis also plays a role in hindlimb skeletal patterning, downstream of *Sall4*. Changes in levels of glycolysis intermediate metabolites are correlated with the presence of hindlimb defects and the absence of forelimb defects in *Sall4* cKO. This result suggests that changes in glycolytic pathway activity are associated with defects in hindlimb development (Akiyama et al., 2015). Moreover, our genetic analysis of *Hk2* provided evidence that *Sall4* regulation of glycolysis contributes to hindlimb skeletal pattern. Our gene expression analysis and ChIP-seq data analysis suggest that SALL4 represses expression of *Hk2*. Since HK2 catalyzes the conversion of glucose to glucose 6-phosphate, the step that occurs at the beginning of glycolysis, *TCre*-mediated inactivation of *Hk2* would have caused restricted glycolysis, which in turn causes reduced levels of intermediates. Similar defects in hindlimb skeleton in *Sall4* cKO and *Hk2* cKO support the idea that *Sall4* regulation of glycolysis controls the development of the proximal-anterior skeleton in hindlimbs.

### *Sall4* regulation of glycolysis in embryos and cancer cells

In the adult body, most cells do not express *Sall4*, and high levels of *Sall4* expression is restricted to oocytes and spermatogonia (Eildermann et al., 2012; Hobbs et al., 2012; Xu et al., 2017). However, many human cancer cells activate expression of *SALL4* (Tatetsu et al., 2016; Zhang et al., 2015). Cancer cells are characterized by aerobic glycolysis or Warburg metabolism, which is associated with increased glucose uptake and lactate production. Contrary to our study, a recent study demonstrated that *SALL4* overexpression promoted and *SALL4* knockdown inhibited glycolysis in human gastric cancer cells (Shao et al., 2020). In gastric cancer cells, overexpression of *SALL4* caused elevation of glucose uptake and lactate production. How *Sall4* cKO in mouse embryos and *SALL4* knockdown in human cancer cells cause opposite effects on glycolysis remains to be elucidated. One possibility is that the cellular context in limb bud cells and gastric cancer cells may cause different regulation of glycolysis by *Sall4*. This idea is consistent with a study of a different type of cancer cells. In human liver cancer cells, it is shown that *SALL4* increases oxidative phosphorylation, oxygen consumption rate, mitochondrial membrane potential, and use of oxidative phosphorylation-related metabolites to generate ATP (Tan et al., 2019). The same study also showed that *SALL4*-expressing liver cancer cells downregulated glycolytic metabolites, which suggested that *SALL4* expression did not initiate Warburg effect. These opposite effects of *SALL4* expression in two types of cancer cells supports the idea that *Sall4* regulation on metabolism is specific to cellular context.

## Supplementary Material

Refer to Web version on PubMed Central for supplementary material.

## Funding

This study was supported by grant from the National Institutes of Health to YK (R01AR064195). The funders had no role in study design, data collection and analysis, decision to publish, or preparation of the manuscript.

### Acknowledgements

We are grateful to Dr. Nissim Hay and Dr. Masayuki Miura for the *Hk2*$^{flox}$ mouse line and the *Aldoa* probe clone, respectively. We are also grateful to Dr. Micah Gearhart, Dr. Naoyuki Tahara, Mr. Calvin Leepalao, Ms. Nhi Huynh and Mr. Justin Wang for their excellent technical support.

## Data availability

RNA-seq and ChIP-seq data have been published (Tahara et al., 2019) and deposited in SRA with BioProject accession number PRJNA525663. All other data will be made available on request.

## References

Akiyama R, Kawakami H, Wong J, Oishi I, Nishinakamura R, Kawakami Y, 2015. Sall4-Gli3 system in early limb progenitors is essential for the development of limb skeletal elements. Proceedings of the National Academy of Sciences of the United States of America 112, 5075–5080. [PubMed: 25848055]

Arora R, Papaioannou VE, 2012. The murine allantois: a model system for the study of blood vessel formation. Blood 120, 2562–2572. [PubMed: 22855605]

Bolger AM, Lohse M, Usadel B, 2014. Trimmomatic: a flexible trimmer for Illumina sequence data. Bioinformatics (Oxford, England) 30, 2114–2120. [PubMed: 24695404]

Brinster RL, 1965. STUDIES ON THE DEVELOPMENT OF MOUSE EMBRYOS IN VITRO. II. THE EFFECT OF ENERGY SOURCE. J Exp Zool 158, 59–68. [PubMed: 14299682]

Bulusu V, Prior N, Snaebjornsson MT, Kuehne A, Sonnen KF, Kress J, Stein F, Schultz C, Sauer U, Aulehla A, 2017. Spatiotemporal Analysis of a Glycolytic Activity Gradient Linked to Mouse Embryo Mesoderm Development. Developmental cell 40, 331–341 e334. [PubMed: 28245920]

Chen KQ, Tahara N, Anderson A, Kawakami H, Kawakami S, Nishinakamura R, Pandolfi PP, Kawakami Y, 2020. Development of the Proximal-Anterior Skeletal Elements in the Mouse Hindlimb Is Regulated by a Transcriptional and Signaling Network Controlled by Sall4. Genetics 215, 129–141. [PubMed: 32156750]

D'Alessandro A, Federica G, Palini S, Bulletti C, Zolla L, 2012. A mass spectrometry-based targeted metabolomics strategy of human blastocoele fluid: a promising tool in fertility research. Molecular bioSystems 8, 953–958. [PubMed: 22020776]

Danecek P, Bonfield JK, Liddle J, Marshall J, Ohan V, Pollard MO, Whitwham A, Keane T, McCarthy SA, Davies RM, Li H, 2021. Twelve years of SAMtools and BCFtools. GigaScience 10.

de Celis JF, Barrio R, 2009. Regulation and function of Spalt proteins during animal development. The International journal of developmental biology 53, 1385–1398. [PubMed: 19247946]

DeBerardinis RJ, Lum JJ, Hatzivassiliou G, Thompson CB, 2008. The biology of cancer: metabolic reprogramming fuels cell growth and proliferation. Cell metabolism 7, 11–20. [PubMed: 18177721]

Eildermann K, Aeckerle N, Debowski K, Godmann M, Christiansen H, Heistermann M, Schweyer S, Bergmann M, Kliesch S, Gromoll J, Ehmcke J, Schlatt S, Behr R, 2012. Developmental expression of the pluripotency factor sal-like protein 4 in the monkey, human and mouse testis: restriction to premeiotic germ cells. Cells, tissues, organs 196, 206–220. [PubMed: 22572102]

Elling U, Klasen C, Eisenberger T, Anlag K, Treier M, 2006. Murine inner cell mass-derived lineages depend on Sall4 function. Proceedings of the National Academy of Sciences of the United States of America 103, 16319–16324. [PubMed: 17060609]

Gándara L, Wappner P, 2018. Metabo-Devo: A metabolic perspective of development. Mechanisms of development 154, 12–23. [PubMed: 29475040]

Heikkinen S, Pietila M, Halmekyto M, Suppola S, Pirinen E, Deeb SS, Janne J, Laakso M, 1999. Hexokinase II-deficient mice. Prenatal death of homozygotes without disturbances in glucose tolerance in heterozygotes. The Journal of biological chemistry 274, 22517–22523. [PubMed: 10428828]

Hobbs RM, Fagoonee S, Papa A, Webster K, Altruda F, Nishinakamura R, Chai L, Pandolfi PP, 2012. Functional antagonism between Sall4 and Plzf defines germline progenitors. Cell Stem Cell 10, 284–298. [PubMed: 22385656]

Jeon H, Lee H, Kang B, Jang I, Roh TY, 2020. Comparative analysis of commonly used peak calling programs for ChIP-Seq analysis. Genomics & informatics 18, e42. [PubMed: 33412758]

Johnson MT, Mahmood S, Patel MS, 2003. Intermediary metabolism and energetics during murine early embryogenesis. The Journal of biological chemistry 278, 31457–31460. [PubMed: 12788927]

Kim D, Paggi JM, Park C, Bennett C, Salzberg SL, 2019. Graph-based genome alignment and genotyping with HISAT2 and HISAT-genotype. Nat Biotechnol 37, 907–915. [PubMed: 31375807]

Kohlhase J, Heinrich M, Liebers M, Frohlich Archangelo L, Reardon W, Kispert A, 2002. Cloning and expression analysis of SALL4, the murine homologue of the gene mutated in Okihiro syndrome. Cytogenet Genome Res 98, 274–277. [PubMed: 12826753]

Kukurugya MA, Titov DV, 2022. The Warburg Effect is the result of faster ATP production by glycolysis than respiration. bioRxiv.

Langmead B, Salzberg SL, 2012. Fast gapped-read alignment with Bowtie 2. Nat Methods 9, 357–359. [PubMed: 22388286]

Leese HJ, 2012. Metabolism of the preimplantation embryo: 40 years on. Reproduction (Cambridge, England) 143, 417–427. [PubMed: 22408180]

Lewis N, Sturmey RG, 2015. Embryo metabolism: what does it really mean? Anim. Reprod 12, 521–528.

Liao Y, Smyth GK, Shi W, 2014. featureCounts: an efficient general purpose program for assigning sequence reads to genomic features. Bioinformatics (Oxford, England) 30, 923–930. [PubMed: 24227677]

Lu C, Thompson CB, 2012. Metabolic regulation of epigenetics. Cell metabolism 16, 9–17. [PubMed: 22768835]

Lu J, Jeong HW, Kong N, Yang Y, Carroll J, Luo HR, Silberstein LE, Yupoma, Chai L, 2009. Stem cell factor SALL4 represses the transcriptions of PTEN and SALL1 through an epigenetic repressor complex. PloS one 4, e5577. [PubMed: 19440552]

McGrath KE, Koniski AD, Malik J, Palis J, 2003. Circulation is established in a stepwise pattern in the mammalian embryo. Blood 101, 1669–1676. [PubMed: 12406884]

Mi H, Muruganujan A, Huang X, Ebert D, Mills C, Guo X, Thomas PD, 2019. Protocol Update for large-scale genome and gene function analysis with the PANTHER classification system (v.14.0). Nat Protoc 14, 703–721. [PubMed: 30804569]

Miller A, Ralser M, Kloet SL, Loos R, Nishinakamura R, Bertone P, Vermeulen M, Hendrich B, 2016. Sall4 controls differentiation of pluripotent cells independently of the Nucleosome Remodelling and Deacetylation (NuRD) complex. Development (Cambridge, England) 143, 3074–3084. [PubMed: 27471257]

Miyazawa H, Yamaguchi Y, Sugiura Y, Honda K, Kondo K, Matsuda F, Yamamoto T, Suematsu M, Miura M, 2017. Rewiring of embryonic glucose metabolism via suppression of PFK-1 and aldolase during mouse chorioallantoic branching. Development (Cambridge, England) 144, 63–73. [PubMed: 28049690]

Nemkov T, Reisz JA, Gehrke S, Hansen KC, D'Alessandro A, 2019. High-Throughput Metabolomics: Isocratic and Gradient Mass Spectrometry-Based Methods. Methods Mol Biol 1978, 13–26. [PubMed: 31119654]

Oginuma M, Harima Y, Tarazona OA, Diaz-Cuadros M, Michaut A, Ishitani T, Xiong F, Pourquié O, 2020. Intracellular pH controls WNT downstream of glycolysis in amniote embryos. Nature 584, 98–101. [PubMed: 32581357]

Oginuma M, Moncuquet P, Xiong F, Karoly E, Chal J, Guevorkian K, Pourquie O, 2017. A Gradient of Glycolytic Activity Coordinates FGF and Wnt Signaling during Elongation of the Body Axis in Amniote Embryos. Developmental cell 40, 342–353 e310. [PubMed: 28245921]

Palsson-McDermott EM, O'Neill LA, 2013. The Warburg effect then and now: from cancer to inflammatory diseases. Bioessays 35, 965–973. [PubMed: 24115022]

Pantier R, Chhatbar K, Quante T, Skourti-Stathaki K, Cholewa-Waclaw J, Alston G, Alexander-Howden B, Lee HY, Cook AG, Spruijt CG, Vermeulen M, Selfridge J, Bird A, 2021. SALL4 controls cell fate in response to DNA base composition. Mol Cell 81, 845–858.e848. [PubMed: 33406384]

Patra KC, Hay N, 2014. The pentose phosphate pathway and cancer. Trends Biochem Sci 39, 347–354. [PubMed: 25037503]

Patra KC, Wang Q, Bhaskar PT, Miller L, Wang Z, Wheaton W, Chandel N, Laakso M, Muller WJ, Allen EL, Jha AK, Smolen GA, Clasquin MF, Robey B, Hay N, 2013. Hexokinase 2 is required for tumor initiation and maintenance and its systemic deletion is therapeutic in mouse models of cancer. Cancer Cell 24, 213–228. [PubMed: 23911236]

Perantoni AO, Timofeeva O, Naillat F, Richman C, Pajni-Underwood S, Wilson C, Vainio S, Dove LF, Lewandoski M, 2005. Inactivation of FGF8 in early mesoderm reveals an essential role in kidney development. Development (Cambridge, England) 132, 3859–3871. [PubMed: 16049111]

Redel BK, Brown AN, Spate LD, Whitworth KM, Green JA, Prather RS, 2012. Glycolysis in preimplantation development is partially controlled by the Warburg Effect. Molecular reproduction and development 79, 262–271. [PubMed: 22213464]

Robinson MD, McCarthy DJ, Smyth GK, 2010. edgeR: a Bioconductor package for differential expression analysis of digital gene expression data. Bioinformatics (Oxford, England) 26, 139–140. [PubMed: 19910308]

Ross-Innes CS, Stark R, Teschendorff AE, Holmes KA, Ali HR, Dunning MJ, Brown GD, Gojis O, Ellis IO, Green AR, Ali S, Chin SF, Palmieri C, Caldas C, Carroll JS, 2012. Differential oestrogen receptor binding is associated with clinical outcome in breast cancer. Nature 481, 389–393. [PubMed: 22217937]

Ru W, Koga T, Wang X, Guo Q, Gearhart MD, Zhao S, Murphy M, Kawakami H, Corcoran D, Zhang J, Zhu Z, Yao X, Kawakami Y, Xu C, 2022. Structural studies of SALL family protein zinc finger cluster domains in complex with DNA reveal preferential binding to an AATA tetranucleotide motif. The Journal of biological chemistry 298, 102607. [PubMed: 36257403]

Sakaki-Yumoto M, Kobayashi C, Sato A, Fujimura S, Matsumoto Y, Takasato M, Kodama T, Aburatani H, Asashima M, Yoshida N, Nishinakamura R, 2006. The murine homolog of SALL4, a causative gene in Okihiro syndrome, is essential for embryonic stem cell proliferation, and cooperates with Sall1 in anorectal, heart, brain and kidney development. Development (Cambridge, England) 133, 3005–3013. [PubMed: 16790473]

Shao M, Zhang J, Zhang J, Shi H, Zhang Y, Ji R, Mao F, Qian H, Xu W, Zhang X, 2020. SALL4 promotes gastric cancer progression via hexokinase II mediated glycolysis. Cancer cell international 20, 188. [PubMed: 32489324]

Solmonson A, Faubert B, Gu W, Rao A, Cowdin MA, Menendez-Montes I, Kelekar S, Rogers TJ, Pan C, Guevara G, Tarangelo A, Zacharias LG, Martin-Sandoval MS, Do D, Pachnis P, Dumesnil D, Mathews TP, Tasdogan A, Pham A, Cai L, Zhao Z, Ni M, Cleaver O, Sadek HA, Morrison SJ, DeBerardinis RJ, 2022. Compartmentalized metabolism supports midgestation mammalian development. Nature 604, 349–353. [PubMed: 35388219]

Sweetman D, Munsterberg A, 2006. The vertebrate spalt genes in development and disease. Developmental biology 293, 285–293. [PubMed: 16545361]

Tahara N, Kawakami H, Chen KQ, Anderson A, Yamashita Peterson M, Gong W, Shah P, Hayashi S, Nishinakamura R, Nakagawa Y, Garry DJ, Kawakami Y, 2019. Sall4 regulates neuromesodermal progenitors and their descendants during body elongation in mouse embryos. Development (Cambridge, England) 146.

Tahara N, Kawakami H, Zhang T, Zarkower D, Kawakami Y, 2018. Temporal changes of Sall4 lineage contribution in developing embryos and the contribution of Sall4-lineages to postnatal germ cells in mice. Sci Rep 8, 16410. [PubMed: 30401915]

Tan JL, Li F, Yeo JZ, Yong KJ, Bassal MA, Ng GH, Lee MY, Leong CY, Tan HK, Wu CS, Liu BH, Chan TH, Tan ZH, Chan YS, Wang S, Lim ZH, Toh TB, Hooi L, Low KN, Ma S, Kong NR, Stein AJ, Wu Y, Thangavelu MT, Suzuki A, Periyasamy G, Asara JM, Dan YY, Bonney GK, Chow EK, Lu GD, Ng HH, Kanagasundaram Y, Ng SB, Tam WL, Tenen DG, Chai L, 2019. New High-Throughput Screening Identifies Compounds That Reduce Viability Specifically in Liver Cancer Cells That Express High Levels of SALL4 by Inhibiting Oxidative Phosphorylation. Gastroenterology 157, 1615–1629.e1617. [PubMed: 31446059]

Tatetsu H, Kong NR, Chong G, Amabile G, Tenen DG, Chai L, 2016. SALL4, the missing link between stem cells, development and cancer. Gene 584, 111–119. [PubMed: 26892498]

Thomas PD, Ebert D, Muruganujan A, Mushayahama T, Albou LP, Mi H, 2022. PANTHER: Making genome-scale phylogenetics accessible to all. Protein science : a publication of the Protein Society 31, 8–22. [PubMed: 34717010]

Tsubooka N, Ichisaka T, Okita K, Takahashi K, Nakagawa M, Yamanaka S, 2009. Roles of Sall4 in the generation of pluripotent stem cells from blastocysts and fibroblasts. Genes Cells 14, 683–694. [PubMed: 19476507]

Vander Heiden MG, Cantley LC, Thompson CB, 2009. Understanding the Warburg effect: the metabolic requirements of cell proliferation. Science (New York, N.Y 324, 1029–1033. [PubMed: 19460998]

Xu K, Chen X, Yang H, Xu Y, He Y, Wang C, Huang H, Liu B, Liu W, Li J, Kou X, Zhao Y, Zhao K, Zhang L, Hou Z, Wang H, Wang H, Li J, Fan H, Wang F, Gao Y, Zhang Y, Chen J, Gao S, 2017. Maternal Sall4 Is Indispensable for Epigenetic Maturation of Mouse Oocytes. The Journal of biological chemistry 292, 1798–1807. [PubMed: 28031467]

Yamamoto T, Takano N, Ishiwata K, Ohmura M, Nagahata Y, Matsuura T, Kamata A, Sakamoto K, Nakanishi T, Kubo A, Hishiki T, Suematsu M, 2014. Reduced methylation of PFKFB3 in cancer cells shunts glucose towards the pentose phosphate pathway. Nat Commun 5, 3480. [PubMed: 24633012]

Zhang J, Tam WL, Tong GQ, Wu Q, Chan HY, Soh BS, Lou Y, Yang J, Ma Y, Chai L, Ng HH, Lufkin T, Robson P, Lim B, 2006. Sall4 modulates embryonic stem cell pluripotency and early embryonic development by the transcriptional regulation of Pou5f1. Nature cell biology 8, 1114–1123. [PubMed: 16980957]

Zhang X, Yuan X, Zhu W, Qian H, Xu W, 2015. SALL4: an emerging cancer biomarker and target. Cancer letters 357, 55–62. [PubMed: 25444934]

## Highlights

- Transcription of glycolytic enzyme genes is upregulated in *Sall4* conditional knockout limb buds.
- SALL4 binds to many genes encoding glycolytic enzymes.
- Levels of glycolytic intermediates are reduced in *Sall4* conditional knockout limb buds.
- *Sall4* restricts glycolysis in limb buds.
- *Hk2* conditional knockout phenocopies hindlimb defects of *Sall4* conditional knockout

A

| Pathway | Number of genes | Fold enrichment | p value | FDR |
|---|---|---|---|---|
| glucose catabolic process (GO:0006007) | 13 | 3.21 | 1.53E-03 | 3.03E-03 |
| hexose catabolic process (GO:0019320) | 17 | 2.72 | 1.45E-03 | 2.92E-03 |
| regulation of glucose import (GO:0046324) | 26 | 2.05 | 2.72E-03 | 4.86E-03 |
| hindlimb morphogenesis (GO:0035137) | 23 | 2.78 | 1.60E-04 | 4.53E-04 |
| limb development (GO:0060173) | 83 | 2.24 | 4.56E-09 | 2.99E-07 |

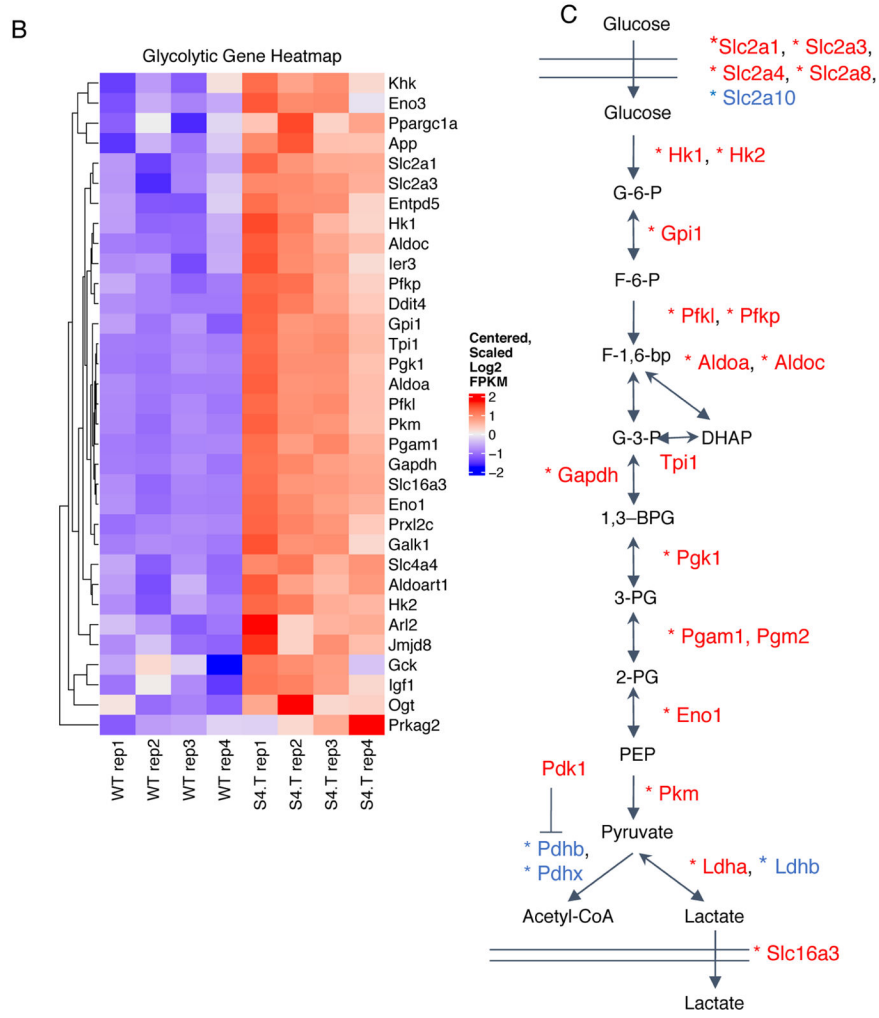


**Figure 1. Upregulation of glycolytic enzyme genes in *Sall4* cKO embryos**

(A) Enrichment of GO terms related to glucose metabolism from differentially expressed genes detected by RNA-seq.

(B) Heatmap of genes related to glucose metabolism. WT, wild type; S4.T, *Sall4* cKO.

(C) Schematic presentation of RNA-seq and ChIP-seq results of genes related to glycolysis. Genes with red and blue fonts are upregulated and downregulated, respectively, in *Sall4* cKO samples, compared to WT samples. Asterisks indicate genes that are bound by SALL4 by SALL4 ChIP-seq. G-6-P: glucose 6-phsphate; 1,3-BPG, 1,3-bisphosphoglycerate; DHAP, dihydroxyacetone phosphate; F-1,6-bp, fructose 1, 6-bisphosphate; F-6-P, fructose 6-phosphate; G-3-P, glyceraldehyde 3-phosphate; G-6-P, glucose 6-phosphate; 2-PG, 2-phosphoglycerate; 3-PG, 3-phosphoglycerate; PEP, phosphoenol pyruvate.

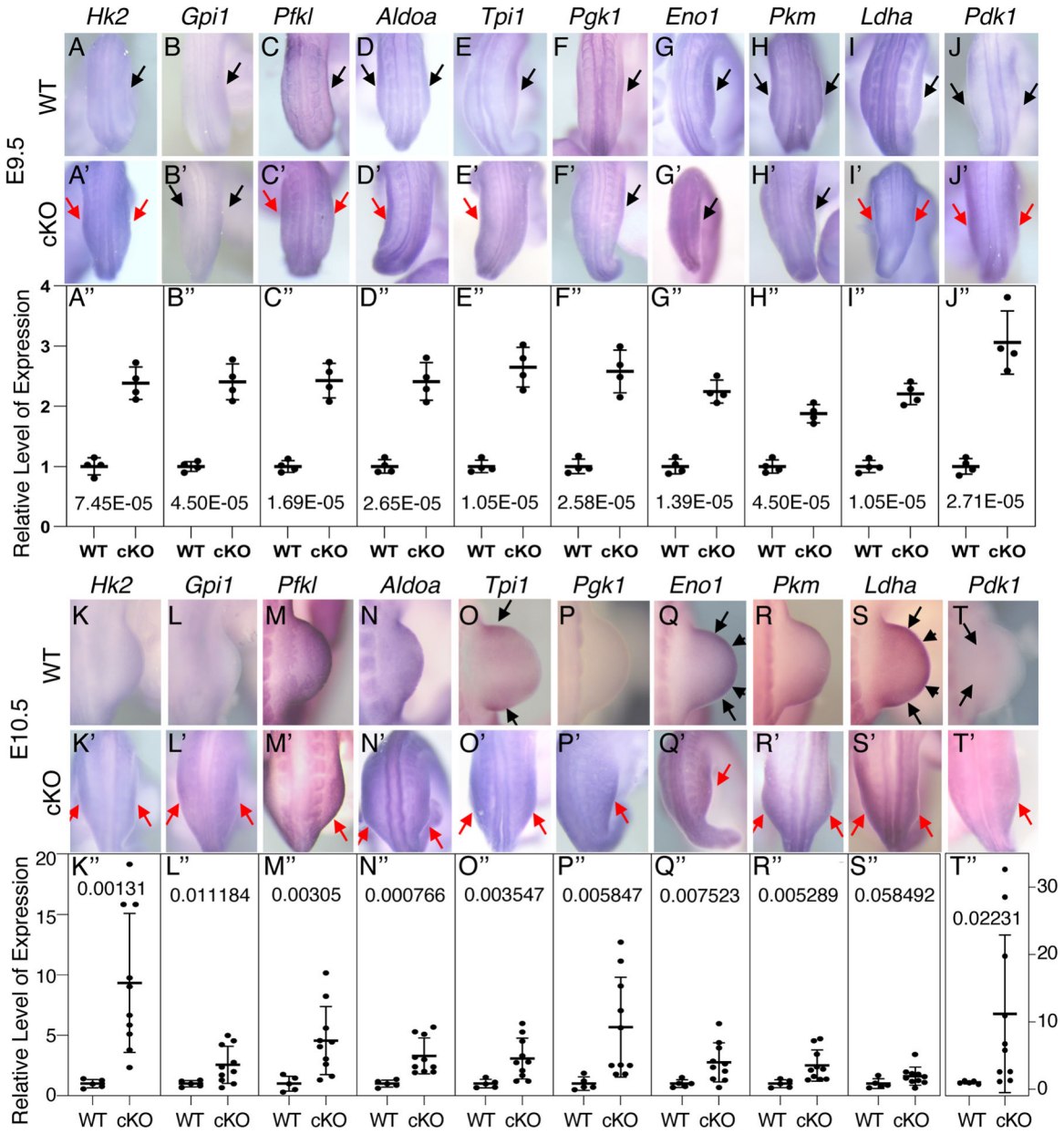


**Figure 2. Expression patterns and levels of glycolytic enzyme genes in the hindlimb-forming region at E9.5 and in the hindlimb bud at E10.5 in WT and *Sall4* cKO embryos**

Dorsal views of expression patterns of *Hk2* (A, A', K, K'), *Gpi1* (B, B', L, L'), *Pfkl* (C, C', M, M'), *Aldoa* (D, D', N, N'), *Tpi1* (E, E', O, O'), *Eno1* (G, G', Q, Q'), *Pkm* (H, H', R, R'), *Ldha* (I, I', S, S'), and *Pkd1* (J, J', T, T') at E9.5 (A-J') and E10.5 (K-T') are shown. Black arrows point to endogenous expression in WT and comparable expression in *Sall4* cKO. Red arrows point to stronger expression in *Sall4* cKO.

Relative expression levels of *Hk2*, *Gpi1*, *Pfkl*, *Aldoa*, *Tpi1*, *Pgk1*, *Eno1*, *Pkm*, *Ldha* and *Pdk1*. A"-J" are generated with the RNA-seq data (n=4 for both WT and *Sall4* cKO), and K"-T" are generated by qRT-PCR (n=5 for WT and n=10 *Sall4* cKO). The average of WT data is set as 1.0. The data in A" to J" have the same y-axis scale shown in A". The data in K" to S" have the same y-axis scale shown in K", and T" has a different y-axis scale shown

in the right side of T". The false discovery rate of RNA-seq data (A"-J") or the p value of *t*-test (K"-T") is shown in each panel.

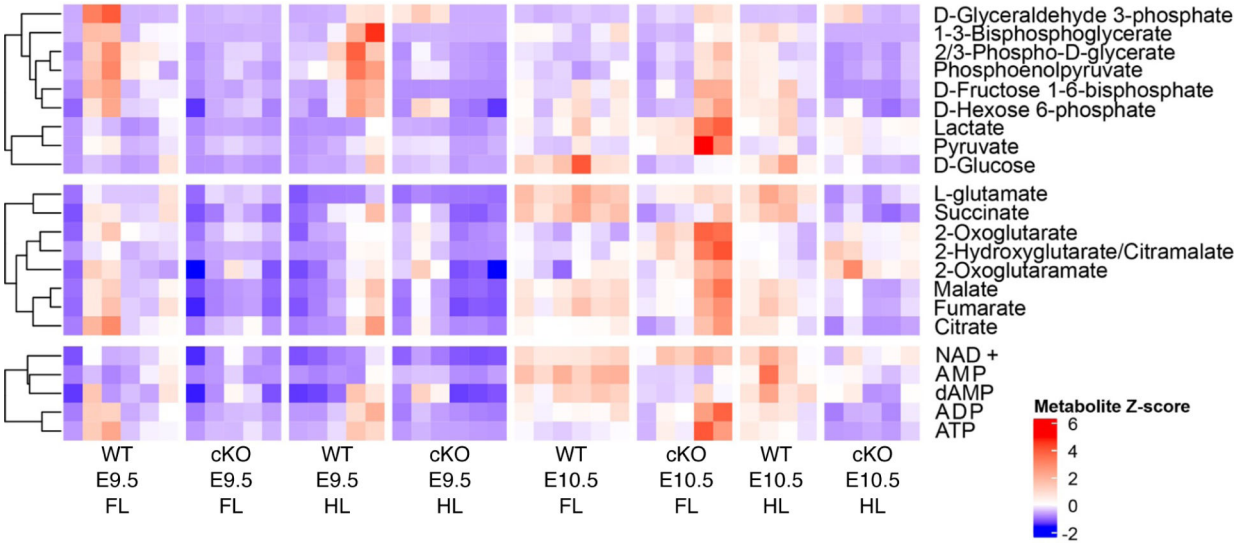


**Figure 3. Heatmap of metabolites in the glycolytic pathway, TCA cycle and energy-related nucleotides.**

Relative levels of metabolites are shown across WT E9.5 forelimb buds, *Sall4* cKO E9.5 forelimb buds, WT E9.5 hindlimb buds, *Sall4* cKO E9.5 hindlimb buds, WT E10.5 forelimb buds, *Sall4* cKO E10.5 forelimb buds, WT E10.5 hindlimb buds, and *Sall4* cKO E10.5 hindlimb buds.

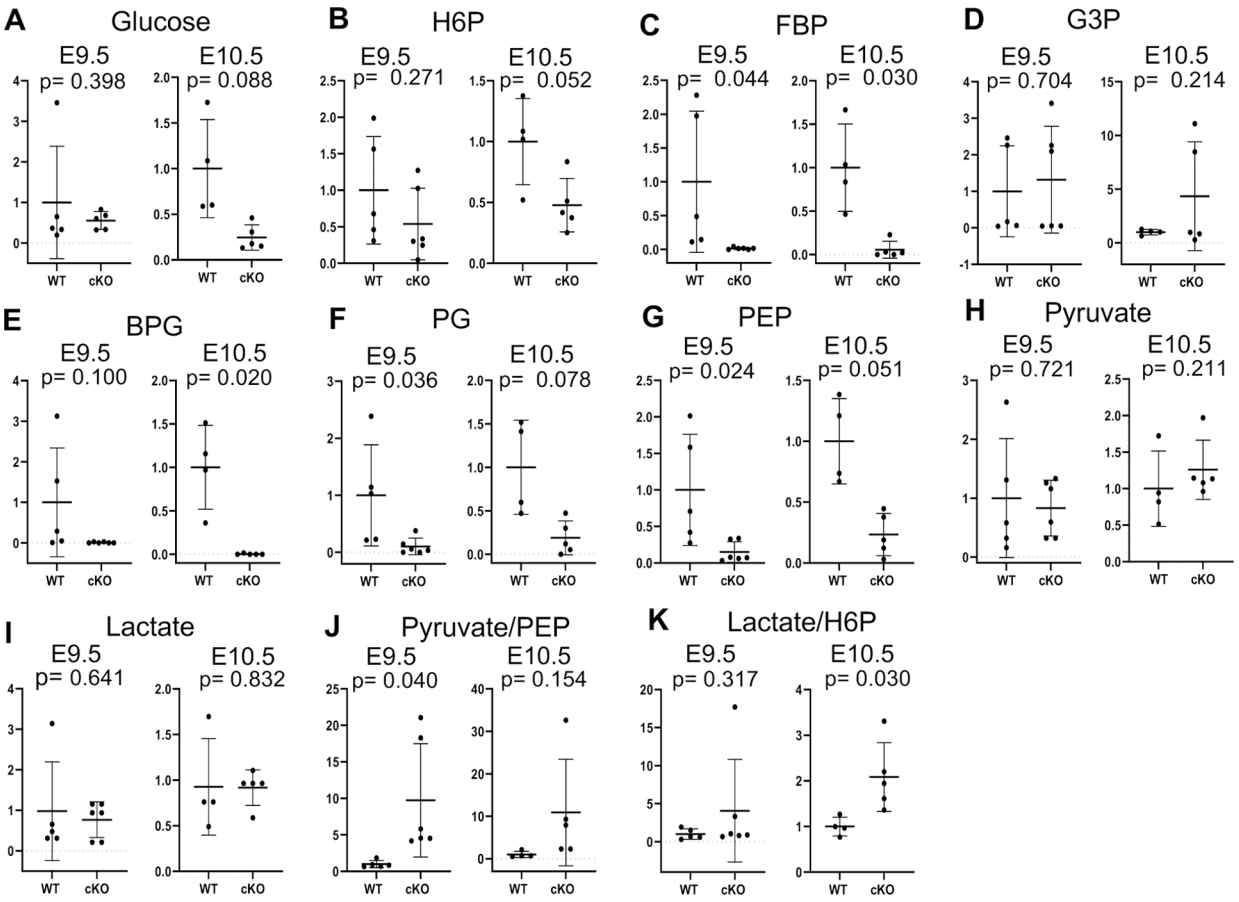


**Figure 4. Reduced levels of glycolytic metabolites in *Sall4* cKO in hindlimb buds**

(A-I) Relative levels of intracellular glucose (A), hexose 6-phosphate (H6P, B), fructose 1,6-bisphosphate (FBP, C), glyceraldehyde 3-phosphate (G3P, D), bisphosphoglycerate (BPG, E), 2/3-Phospho-D-glycerate (PG, F), phosphoenol pyruvate (PEP, G), pyruvate (H), lactate (I) at E9.5 and E10.5.

(J, K) Ratios of pyruvate/phosphoenol pyruvate (J) and lactate/hexose 6-phosphate (K) at E9.5 and E10.5.

Each dot represents a sample, and bars show average ± standard deviation. Statistical test was performed by unpaired *t*-test and the p-values are shown in each panel.

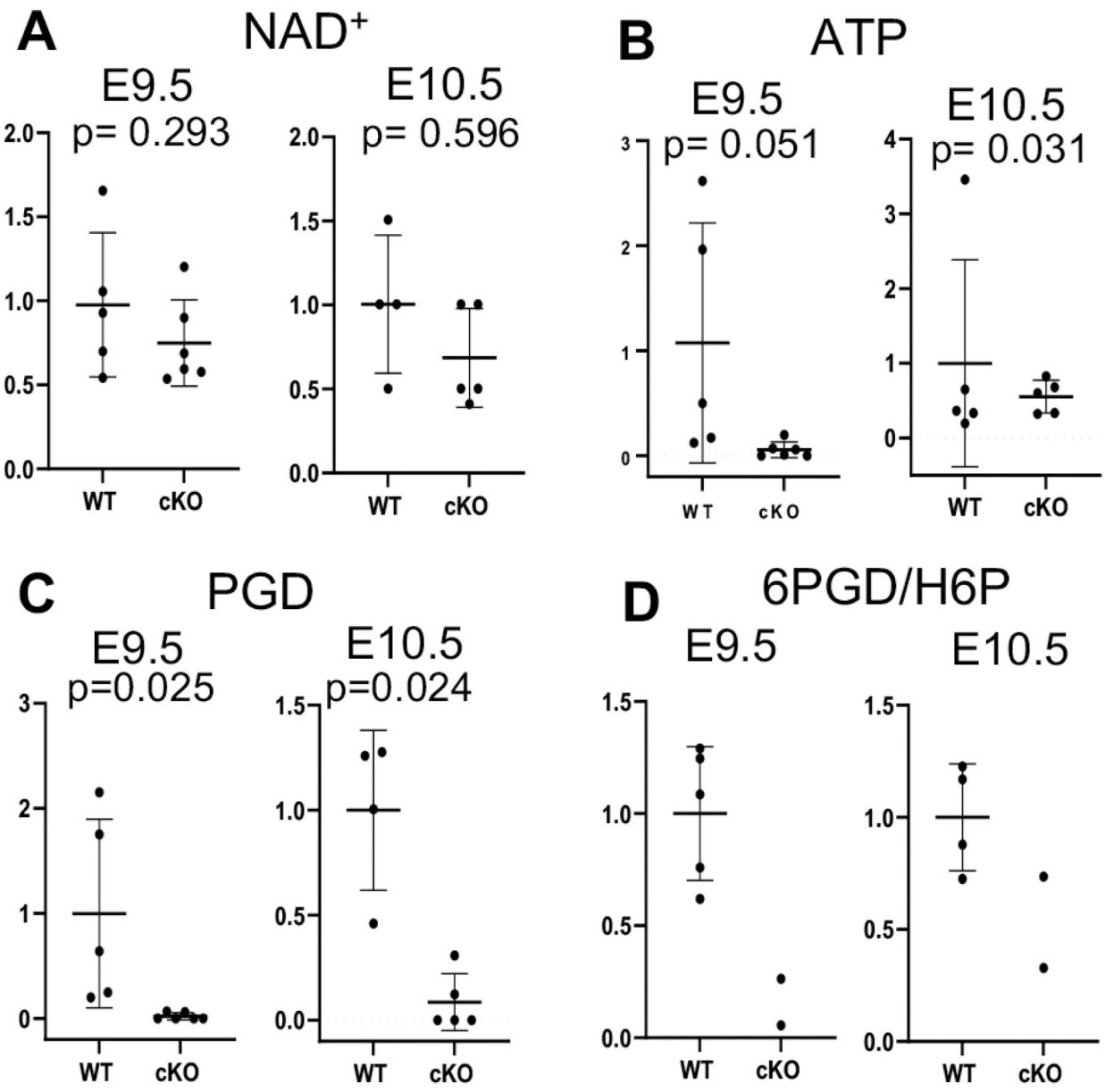


**Figure 5. Reduced levels of NAD+, ATP and 6-Phospho-D-gluconate in *Sall4* cKO hindlimb buds**

(A-C) Relative levels of $NAD^+$ (A), ATP (B), and 6-phospho-D-gluconate (PGD, C) at E9.5 and E10.5.

(D) Ratios of 6-phospho-D-gluconate/hexose 6-phosphate at E9.5 and E10.5. The 6-phospho-D-gluconate value was 0 for 4 E9.5 cKO and 3 E10.5 cKO samples, which are excluded from the ratio analysis. The sample size is n=2 for both E9.5 cKO and E10.5 cKO. Each dot represents a sample, and bars show average ± standard deviation. Statistical test was performed by unpaired *t*-test and the p-values are shown in each panel.

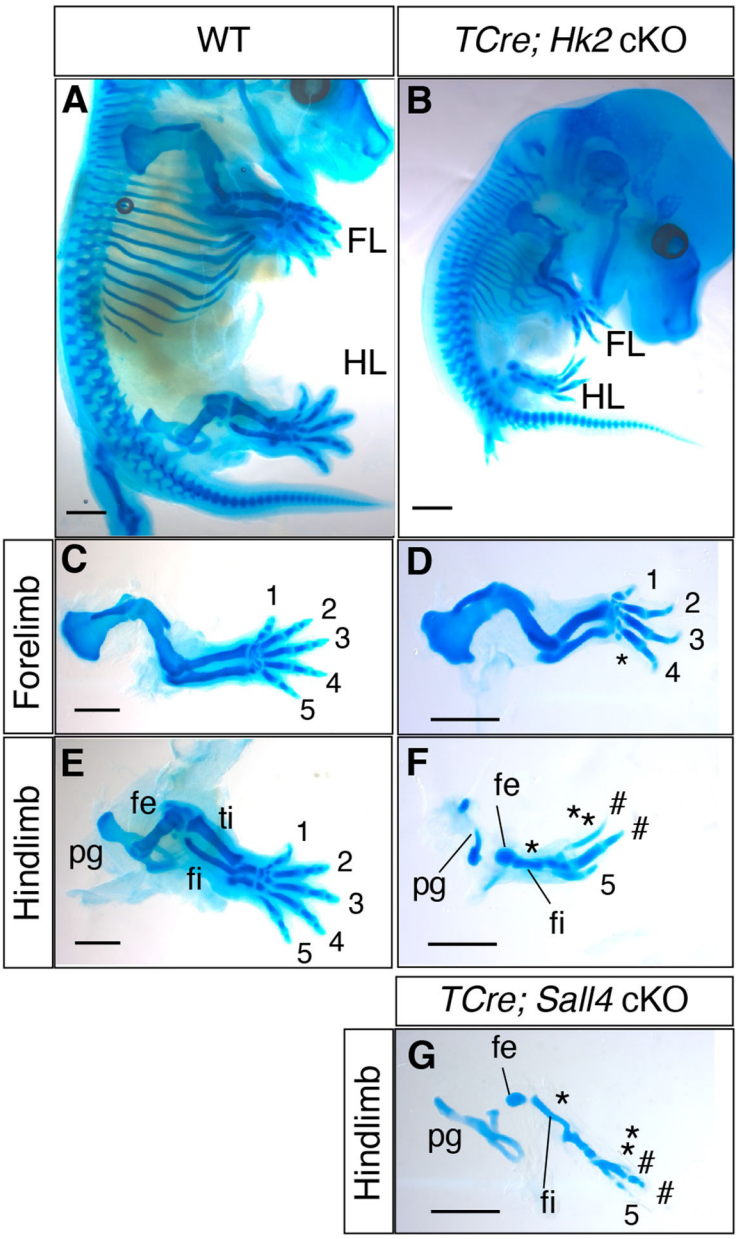


**Figure 6. *Hk2* cKO hindlimbs exhibit defects similar to *Sall4* cKO hindlimbs**

Alcian blue-stained WT (A, C, E), *TCre Hk2* cKO (B, D, F) and *TCre; Sall4* cKO (G) skeleton at E14.5. A and B are on the same scale. Close ups of the forelimb (C, D) and hindlimb (E-G) are shown. The pound (#) marks the tip of digits whose identity is not unknown. Digits are labelled with 1–5. The asterisk (*) labels the area where a skeletal element is missing. Abbreviation: fe: femur, fi: fibula, FL: forelimb, HL: hindlimb, pg: pelvic girdle, ti: tibia. Scale bar, 1 mm. Note panels D, F, G are at different magnification compared to panels C and E.

**Table 1**

Summary of limb skeletal phenotype of *TCre; Hk2* cKO embryos

| | | WT | *Hk2* cKO |
|---|---|---|---|
| Femur | Normal | 30 | 0 |
| | Small condensation | 0 | 12 (100%) |
| Tibia | Normal | 30 | 0 |
| | Missing | 0 | 12 (100%) |
| Digit number | 5 | 30 | 0 |
| (hindlimb) | 4 | 0 | 8 (67%) |
| | 3 | 0 | 4 (32%) |
| Digit number | 5 | 30 | 6 (50%) |
| (forelimb) | 4 | 0 | 2 (17%) |
| | 3 | 0 | 3 (25%) |
| | 2 | 0 | 1 (8%) |

Indicated are number of limbs. Normal indicates normal morphology without missing or severely malformed parts.